INTERNATIONAL JOURNAL FOR NUMERICAL METHODS IN FLUIDS
Int. J. Numer. Meth. Fluids **26**: 887–905 (1998)

CALCULATION OF LAMINAR FLOWS WITH SECOND-ORDER SCHEMES AND COLLOCATED VARIABLE ARRANGEMENT

FERNANDO BIAGIOLI

CRS4-Centre for Advanced Studies, Research and Development in Sardinia, Via N. Sauro, 10-09123 Cagliari, Italy

SUMMARY

A numerical study of laminar flows is carried out to examine the performance of two second-order discretization schemes: a total variation diminishing scheme and a second-order upwind scheme. The former has the same form as the standard first-order hybrid central upwind scheme, but with a numerical diffusion reduced by the Van Leer limiter; the latter is based on the linear extrapolation of cell face values using the two upwind neighbors. A collocated grid arrangement is used; oscillations which could be generated by pressure–velocity decoupling are avoided via the Rhie–Chow interpolation. Two iterative solution methods are used: (i) the deferred correction procedure proposed by Khosla and Rubin and (ii) implicit treatment of the second-order upwind contribution. Three two-dimensional laminar test cases are considered for assessment: the plane lid-driven cavity, the plane backward facing step and the axisymmetric pipe with sudden contraction. Experimental data are available for the two last cases. Both the total variation diminishing and the second-order upwind schemes give wiggle-free results and can predict the flowfields more accurately than the standard first-order hybrid central upwind scheme. © 1998 John Wiley & Sons, Ltd.

KEY WORDS: laminar flows; incompressible flows; second-order schemes

1. INTRODUCTION

The accuracy of numerical predictions in computational fluid dynamics (CFD) may be significantly affected by the discretization scheme chosen for the convective terms. The classical hybrid central upwind scheme (CU) [1] is only first-order-accurate and therefore introduces excessive numerical diffusion in flows which are dominated by convection.

Several second-order-accurate schemes have been developed during the last 20 years, such as the quadratic-upstream interpolation for convective kinematics scheme (QUICK) [2] and the second-order upwind scheme (SOU) [3]. The simple model problem analysis indicates that these schemes are prone to numerical oscillations ('overshoots' and 'undershoots'), therefore, modified versions of the QUICK scheme [4,5] and second-order total variation diminishing schemes [6,7] (TVD) which are free of numerical oscillations have been developed. The application of TVD schemes has been limited mainly to supersonic flows, where sharp gradients associated with shock waves must be captured, while their use for incompressible flows has recently been proposed by Jones [8] for the simulation of low Mach number turbulent combustion problems. Their implementation is straightforward, starting from the CU scheme as their founding lies on the limitation via a flux limiter [9,10] of the first-order upwind numerical diffusion.

CCC 0271–2091/98/080887–19$17.50

Received June 1996
Revised May 1997

In this work, the SOU and TVD schemes were implemented in a multiblock code developed by the author [11], based on a collocated grid arrangement (no staggering). They were tested on three two-dimensional laminar test cases: the plane lid-driven cavity, the plane backward facing step (recirculating flows) and the axisymmetric pipe with sudden contraction.

The main difficulty encountered when implementing second-order schemes is that the coefficient matrix obtained from the quasi-linear approximation of the discretized equations may loose its diagonal dominance for the case of convection-dominated flows, and stability problems may arise during the iterative solution of the Navier–Stokes equations. This is the case for e.g. the TVD scheme, unless very small relaxation parameters in the momentum equation are used; on the contrary, the CU scheme always ensures a diagonally-dominant coefficient matrix.

In order to obtain a diagonally-dominant coefficient matrix during the iterative solution of the incompressible Navier–Stokes equations, the deferred correction method originally proposed by Khosla and Rubin [12] was used here with the TVD and SOU schemes. According to this method a numerical scheme characterized by a diagonally-dominant coefficient matrix (e.g. the CU or a fully upwind scheme) is solved implicitly, while the extra deferred correction term of the second-order scheme is treated as an explicit source.

The results obtained in this study using the CU, TVD and SOU schemes were compared with the numerical results of Ghia *et al.* [13] for the plane lid-driven cavity flow, the experiments by Armaly *et al.* [14] for the plane backward facing step and the experiments by Durst and Loy [15] for the axisymmetric pipe with sudden contraction.

The objective of the present work is twofold:

1. to assess the performance of the TVD and SOU schemes with respect to the CU scheme;
2. to identify, on the basis of the tests performed, advantages and disadvantages of the Khosla and Rubin deferred correction method.

2. GOVERNING EQUATIONS

The governing equations for two-dimensional, incompressible, steady laminar flows can be written in a Cartesian-cylindrical co-ordinate system as follows:

continuity equation

$$\frac{\partial u}{\partial x}+\frac{1}{y^j}\frac{\partial (y^j v)}{\partial y}=0, \tag{1}$$

momentum equations

$$\frac{\partial}{\partial x}(uu)+\frac{1}{y^j}\frac{\partial}{\partial y}(y^j uv)=-\frac{1}{\rho}\frac{\partial p}{\partial x}+\nu\left[\frac{\partial^2 u}{\partial x^2}+\frac{1}{y^j}\frac{\partial}{\partial y}\left(y^j\frac{\partial u}{\partial y}\right)\right], \tag{2}$$

$$\frac{\partial}{\partial x}(uv)+\frac{1}{y^j}\frac{\partial}{\partial y}(y^j vv)=-\frac{1}{\rho}\frac{\partial p}{\partial y}+\nu\left[\frac{\partial^2 v}{\partial x^2}+\frac{1}{y^j}\frac{\partial}{\partial y}\left(y^j\frac{\partial v}{\partial y}\right)-2j\frac{v}{y^{2j}}\right], \tag{3}$$

where $j=0$ applies to plane cases and $j=1$ to axisymmetric cases. In these equations u and v are the velocity components in the x- and y-directions respectively, ρ is the density, p the pressure and ν the kinematic viscosity.

3. NUMERICAL METHOD

The momentum equations are discretized with the finite volume method based on a collocated grid arrangement (non-staggered grid) shown schematically in Figure 1.

The diffusive terms are discretized by central differencing. The convective terms are discretized here by three different schemes: the first-order hybrid central upwind CU scheme, a hybrid central-TVD scheme (globally second-order-accurate) and the second-order upwind SOU scheme.

In the case of CU and TVD schemes the convective plus diffusive flux for the generic variable (e.g. at the east boundary) is set as:

$$\left[u\phi - v\frac{\partial\phi}{\partial x}\right]_e \simeq u_e\frac{\phi_E+\phi_P}{2} - \Gamma_e\frac{\phi_E-\phi_P}{x_E-x_P}, \tag{4}$$

where the diffusion coefficient Γ_e depends on the face Peclet number $Pe_e = |u_e|(x_E - x_P)/v$:

$$\Gamma_e = v, \quad \text{if} \quad Pe_e \le 2, \tag{5}$$

$$\Gamma_e = \max\left[v, \frac{|u|_e}{2}(1-\psi_e)(x_E-x_P)\right], \quad \text{if} \quad Pe_e > 2, \tag{6}$$

ψ_e being a numerical diffusion limiter assumed equal to zero in the case of the CU scheme and equal to the Van Leer limiter [10] in the case of the TVD scheme. In the last case, the expression for ψ_e is given by:

$$\psi_e = \frac{r_e + |r_e|}{1+r_e},$$

$$r_e = \frac{\phi_P - \phi_W}{\phi_E - \phi_P}, \qquad u_e \ge 0,$$

$$r_e = \frac{\phi_E - \phi_{EE}}{\phi_P - \phi_E}, \qquad u_e < 0. \tag{7}$$

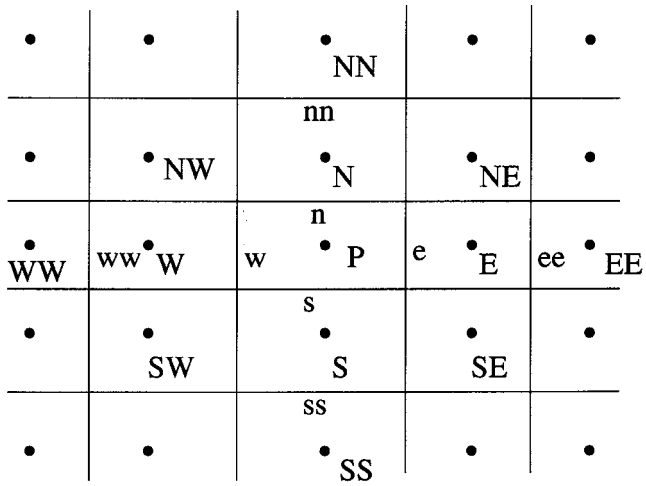

Figure 1. Finite volume grid.

Similar expressions hold for the west, north and south faces. These schemes are of the hybrid type: central differencing is used for $Pe \leq 2$, and upwinding for $Pe > 2$. For $Pe > 2$, the physical diffusion term is omitted in order to ensure continuity with the central difference scheme used for $Pe \leq 2$.

In the SOU scheme the convective flux for the generic variable ϕ (e.g. at the east boundary) is calculated assuming a linear interpolation between the two upstream nodes:

$$[u\phi]_e = \frac{(u+|u|)_e}{2}(1.5\phi_P - 0.5\phi_W) + \frac{(u-|u|)_e}{2}(1.5\phi_E - 0.5\phi_{EE}). \tag{8}$$

Also in this case, similar expressions hold for the west, north and south faces.

The conservation Equations (2) and (3) for the momentum components are cast in the form:

$$A_P u_P = \sum_{NB=E,W,N,S} A_{NB} u_{NB} - \frac{S_e + S_w}{2}\frac{p_E - p_W}{2} + Q_P \tag{9}$$

$$A_P v_P = \sum_{NB=E,W,N,S} A_{NB} v_{NB} - \frac{S_n + S_s}{2}\frac{p_N - p_S}{2} - 2jv\frac{v_P}{y_P^{2j}}V_P + Q_P \tag{10}$$

where S_e, S_w, S_n, S_s are the east, west, north and south cell faces surfaces, V_P the cell volume and Q_P is the extra deferred correction term. A $2-\Delta x$ central differences discretization of the pressure gradient components was used in these equations.

The iterative solution algorithm is based on the SIMPLE method [1]; the step from iteration (n) to iteration $(n+1)$ can be summarized as follows:

- The velocity components u^*, v^* are guessed at an intermediate iteration, solving the following equations in relaxed form:

$$A_P u_P^* = r_u\left[\sum_{NB=E,W,N,S} A_{NB} u_{NB}^* - \frac{S_e + S_w}{2}\frac{p_E^{(n)} - p_W^{(n)}}{2} + Q_P^{(n)}\right] + (1-r_u)A_P u_P^{(n)}, \tag{11}$$

$$A_P v_P^* = r_v\left[\sum_{NB=E,W,N,S} A_{NB} v_{NB}^* - \frac{S_n + S_s}{2}\frac{p_N^{(n)} - p_S^{(n)}}{2} - 2vj\frac{v_P^{(n)}}{r_P^{2j}}V_P + Q_P^{(n)}\right] + (1-r_v)A_P v_P^{(n)} \tag{12}$$

  where the purpose of the relaxation parameters is to improve convergence by limiting the velocity variations.
- The velocity components at the iteration step $(n+1)$ are obtained from the relations

$$u_P^{(n+1)} = u_P^* - \frac{1}{A_P}\frac{S_e + S_w}{2}\frac{\delta p_E^{(n+1)} - \delta p_W^{(n+1)}}{2}, \tag{13}$$

$$v_P^{(n+1)} = v_P^* - \frac{1}{A_P}\frac{S_n + S_s}{2}\frac{\delta p_N^{(n+1)} - \delta p_S^{(n+1)}}{2}, \tag{14}$$

  where $\delta p^{(n+1)} = p^{(n+1)} - p^{(n)}$ is the pressure increment between two consecutive iterations.
- The algebraic relations (13) and (14) are inserted in the mass conservation Equation (1) integrated over the finite volume:

$$u_e^{(n+1)}S_e - u_w^{(n+1)}S_w + v_n^{(n+1)}S_n - v_s^{(n+1)}S_s = 0. \tag{15}$$

  In order to avoid pressure–velocity decoupling, the velocity components on cell boundaries are calculated using the Rhie–Chow interpolation method [16], i.e. according to the linear interpolation of the velocity values u^* (v^*) in the two nodes adjacent to the boundary, each of them purified by the $2-\Delta x(2-\Delta r)$ pressure gradient contribution and incremented with

the $1-\Delta x$ $(1-\Delta r)$ contribution between the two adjacent nodes; e.g. at the east boundary such interpolation at iteration $(n+1)$ yields:

$$u_{\mathrm{e}}^{(n+1)} = \frac{u_{\mathrm{P}}^{*} + u_{\mathrm{E}}^{*}}{2} - \frac{1}{2}\frac{S_{\mathrm{e}} + S_{\mathrm{w}}}{2}\left[-\frac{r_u}{A_{\mathrm{P}}}\frac{p_{\mathrm{E}}^{(n)} - p_{\mathrm{W}}^{(n)}}{2}\right] - \frac{1}{2}\frac{S_{\mathrm{e}} + S_{\mathrm{ee}}}{2}\left[-\frac{r_u}{A_{\mathrm{P_E}}}\frac{p_{\mathrm{EE}}^{(n)} - p_{\mathrm{P}}^{(n)}}{2}\right] - \left(\frac{r_u}{A_{\mathrm{P}}}\right)_{\mathrm{e}} S_{\mathrm{e}}(p_{\mathrm{E}}^{(n+1)} - p_{\mathrm{P}}^{(n+1)}), \tag{16}$$

where $1/A_{\mathrm{P_E}}$ and $(1/A_{\mathrm{P}})_{\mathrm{e}}$ represent the inverse of the A_{P} coefficient at the east node and east face, respectively. The velocity components calculated in Equation (16) are introduced into Equation (15), giving the following Poisson-type equation for the pressure correction:

$$-a_{\mathrm{P}}\delta p_{\mathrm{P}}^{(n+1)} + \sum_{NB=\mathrm{E,W,N,S}} a_{NB}\delta p_{NB}^{(n+1)} = -\dot{m}^{*}, \tag{17}$$

where the coefficients and the mass defect term are given by:

$$a_{\mathrm{E}} = r_u\frac{S_{\mathrm{e}}}{2}\left(\frac{1}{A_{\mathrm{E}}} + \frac{1}{A_{\mathrm{P}}}\right), \qquad a_{\mathrm{W}} = r_u\frac{S_{\mathrm{w}}}{2}\left(\frac{1}{A_{\mathrm{W}}} + \frac{1}{A_{\mathrm{P}}}\right), \tag{18}$$

$$a_{\mathrm{N}} = r_v\frac{S_{\mathrm{n}}}{2}\left(\frac{1}{A_{\mathrm{N}}} + \frac{1}{A_{\mathrm{P}}}\right), \qquad a_{\mathrm{S}} = r_v\frac{S_{\mathrm{s}}}{2}\left(\frac{1}{A_{\mathrm{S}}} + \frac{1}{A_{\mathrm{P}}}\right), \tag{19}$$

$$a_{\mathrm{P}} = \sum_{NB=\mathrm{E,W,N,S}} a_{NB} \tag{20}$$

$$\dot{m}^{*} = u_{\mathrm{e}}^{*}S_{\mathrm{e}} - u_{\mathrm{w}}^{*}S_{\mathrm{w}} + u_{\mathrm{n}}^{*}S_{\mathrm{n}} - u_{\mathrm{s}}^{*}S_{\mathrm{s}}. \tag{21}$$

The use of a non-staggered grid arrangement is more convenient than the staggered grid, because it leads to a simpler and more efficient formulation of the boundary conditions, especially in the case of a multiblock code such as the one used in this work.

- Finally, the momentum and pressure correction equations are solved iteratively using a tridiagonal matrix algorithm (TDMA) until convergence is achieved, i.e. the total mass and momentum residuals are below a prescribed tolerance.

The expressions for the coefficients A_{P}, A_{NB} depends upon the discretization scheme used. In the cases of the CU and TVD schemes these coefficients are given by:

$$A_{\mathrm{E}} = \left[\frac{\max[v, \Gamma_{\mathrm{e}}]}{x_{\mathrm{E}} - x_{\mathrm{P}}} - \frac{1}{2}u_{\mathrm{e}}\right]S_{\mathrm{e}}, \tag{22}$$

$$A_{\mathrm{W}} = \left[\frac{\max[v, \Gamma_{\mathrm{w}}]}{x_{\mathrm{P}} - x_{\mathrm{W}}} + \frac{1}{2}u_{\mathrm{w}}\right]S_{\mathrm{w}}, \tag{23}$$

$$A_{\mathrm{N}} = \left[\frac{\max[v, \Gamma_{\mathrm{n}}]}{r_{\mathrm{N}} - r_{\mathrm{P}}} - \frac{1}{2}v_{\mathrm{n}}\right]S_{\mathrm{n}}, \tag{24}$$

$$A_{\mathrm{S}} = \left[\frac{\max[v, \Gamma_{\mathrm{s}}]}{r_{\mathrm{P}} - r_{\mathrm{S}}} + \frac{1}{2}v_{\mathrm{s}}\right]S_{\mathrm{s}}, \tag{25}$$

$$A_{\mathrm{P}} = A_{\mathrm{E}} + A_{\mathrm{W}} + A_{\mathrm{N}} + A_{\mathrm{S}}, \qquad Q_{\mathrm{P}} = 0, \tag{26}$$

where the diffusion coefficients Γ_{nb}, $nb = \mathrm{e, w, n, s}$ are given by Equation (5) or (6) according to the face Peclet number. It is not difficult to verify that the condition of a diagonally-dominant coefficient matrix given by:

$$|A_{\mathrm{P}}| \geq \sum_{NB} |A_{NB}| \tag{27}$$

is always satisfied by the CU scheme, but not by the TVD scheme. This is due to the fact that the off-diagonal coefficients can be negative in the case of convection-dominated flows, therefore stability problems could arise in the last case during the numerical solution of the Navier–Stokes equations.

In order to have an iterative solution method based on a diagonally-dominant coefficient matrix when using the TVD scheme aswell, two different methods were adopted. The first of these methods is represented by Khosla and Rubin's deferred correction procedure; in this case the A_{NB} coefficients are set as in Equations (22)–(25) assuming $\psi_{nb} = 0$ (which corresponds to the CU scheme) and the deferred correction term Q_{P} (treated explicitly) is given, for instance at the east face, by:

$$Q_{\mathrm{P}} = 0 \quad \text{if} \quad Pe_{\mathrm{e}} \leq 2, \tag{28}$$

$$Q_{\mathrm{P}} = -\frac{|u_{\mathrm{e}}|}{2}(x_{\mathrm{E}} - x_{\mathrm{P}})\psi_{\mathrm{e}} \frac{\phi_{\mathrm{E}} - \phi_{\mathrm{P}}}{x_{\mathrm{E}} - x_{\mathrm{P}}} S_{\mathrm{ew}} \quad \text{if} \quad Pe_{\mathrm{e}} > 2 \quad \text{and} \quad (1 - \psi_{\mathrm{e}}) \frac{|u_{\mathrm{e}}|}{2}(x_{\mathrm{E}} - x_{\mathrm{P}}) > v, \tag{29}$$

$$Q_{\mathrm{P}} = \left[-\frac{|u_{\mathrm{e}}|}{2}(x_{\mathrm{E}} - x_{\mathrm{P}}) + v \right] \frac{\phi_{\mathrm{E}} - \phi_{\mathrm{P}}}{x_{\mathrm{E}} - x_{\mathrm{P}}} S_{\mathrm{ew}} \quad \text{if} \quad Pe_{\mathrm{e}} > 2 \quad \text{and} \quad (1 - \psi_{\mathrm{e}}) \frac{|u_{\mathrm{e}}|}{2}(x_{\mathrm{E}} - x_{\mathrm{P}}) < v. \tag{30}$$

The second method increases the diagonal dominance of the coefficient matrix by employing small values for the relaxation parameters r_u and r_v; e.g. the coefficient matrix obtained incorporating expressions Equations (22)–(26) for the case of the TVD scheme in Equations (11) and (12) can be made diagonally-dominant by using relaxation parameters which are continuously updated every iteration and such that the condition

$$|A_{\mathrm{P}}| \geq r \sum_{NB} |A_{NB}| \tag{31}$$

is satisfied over the whole flowfield.

The following implementation, where as many terms as possible are treated implicitly to give a diagonally-dominant coefficient matrix, was instead adopted for the SOU scheme:

$$A_{\mathrm{N}} = \left[\frac{v}{y_{\mathrm{N}} - y_{\mathrm{P}}} - \frac{1}{2}\left(\frac{1}{2}(v_{\mathrm{s}} - |v_{\mathrm{s}}|) + (v_{\mathrm{n}} - |v_{\mathrm{n}}|) \right) \right] S_{\mathrm{ns}}, \tag{32}$$

$$A_{\mathrm{S}} = \left[\frac{v}{y_{\mathrm{P}} - y_{\mathrm{S}}} + \frac{1}{2}\left(\frac{1}{2}(|v_{\mathrm{n}}| + v_{\mathrm{n}}) + (|v_{\mathrm{s}}| + v_{\mathrm{s}}) \right) \right] S_{\mathrm{ns}}, \tag{33}$$

$$A_{\mathrm{E}} = \left[\frac{v}{x_{\mathrm{E}} - x_{\mathrm{P}}} - \frac{1}{2}\left(\frac{1}{2}(u_{\mathrm{w}} - |u_{\mathrm{w}}|) + (u_{\mathrm{e}} - |u_{\mathrm{e}}|) \right) \right] S_{\mathrm{ew}}, \tag{34}$$

$$A_{\mathrm{W}} = \left[\frac{v}{x_{\mathrm{P}} - x_{\mathrm{W}}} + \frac{1}{2}\left(\frac{1}{2}(|u_{\mathrm{e}}| + u_{\mathrm{e}}) + (|u_{\mathrm{w}}| + u_{\mathrm{w}}) \right) \right] S_{\mathrm{ew}}, \tag{35}$$

$$A_{\mathrm{P}} = A_{\mathrm{E}} + A_{\mathrm{W}} + A_{\mathrm{S}} + A_{\mathrm{N}}, \tag{36}$$

$$Q_{\mathrm{P}} = \frac{1}{4}\{[(|u_{\mathrm{e}}| - u_{\mathrm{e}})(\phi_{\mathrm{E}} - \phi_{\mathrm{EE}}) + (|u_{\mathrm{w}}| + u_{\mathrm{w}})(\phi_{\mathrm{W}} - \phi_{\mathrm{WW}})] S_{\mathrm{ew}} + [(|v_{\mathrm{n}}| - v_{\mathrm{n}})(\phi_{\mathrm{N}} - \phi_{\mathrm{NN}}) + (|v_{\mathrm{s}}| + v_{\mathrm{s}})(\phi_{\mathrm{S}} - \phi_{\mathrm{SS}})] S_{\mathrm{ns}}\}. \tag{37}$$

This implementation of the SOU scheme gives a diagonally-dominant matrix; in fact, the coefficients A_{NB} are always positive.

Moreover, the Khosla and Rubin method has been implemented in this case. The coefficients are given by:

$$A_{\mathrm{N}} = \left[\left(\frac{|v_{\mathrm{n}}|}{2} + \frac{v}{y_{\mathrm{N}} - y_{\mathrm{P}}}\right) - \frac{v_{\mathrm{n}}}{2}\right] S_{\mathrm{ns}}, \tag{38}$$

$$A_{\mathrm{S}} = \left[\left(\frac{|v_{\mathrm{s}}|}{2} + \frac{v}{y_{\mathrm{P}} - y_{\mathrm{S}}}\right) + \frac{v_{\mathrm{s}}}{2}\right] S_{\mathrm{ns}}, \tag{39}$$

$$A_{\mathrm{E}} = \left[\left(\frac{|u_{\mathrm{e}}|}{2} + \frac{v}{x_{\mathrm{E}} - x_{\mathrm{P}}}\right) - \frac{u_{\mathrm{e}}}{2}\right] S_{\mathrm{ew}}, \tag{40}$$

$$A_{\mathrm{W}} = \left[\left(\frac{|u_{\mathrm{w}}|}{2} + \frac{v}{x_{\mathrm{P}} - x_{\mathrm{W}}}\right) + \frac{u_{\mathrm{w}}}{2}\right] S_{\mathrm{ew}}, \tag{41}$$

$$A_{\mathrm{P}} = A_{\mathrm{E}} + A_{\mathrm{W}} + A_{\mathrm{S}} + A_{\mathrm{N}}, \tag{42}$$

$$\begin{aligned} Q_{\mathrm{P}} = \frac{1}{2}\Bigg\{ & \left[\frac{|u_{\mathrm{w}}| + u_{\mathrm{w}}}{2}(\phi_{\mathrm{W}} - \phi_{\mathrm{WW}}) + \frac{u_{\mathrm{w}} - |u_{\mathrm{w}}|}{2}(\phi_{\mathrm{P}} - \phi_{\mathrm{E}}) + \frac{|u_{\mathrm{e}}| - u_{\mathrm{e}}}{2}(\phi_{\mathrm{E}} - \phi_{\mathrm{EE}})\right. \\ & \left. + \frac{|u_{\mathrm{e}}| + u_{\mathrm{e}}}{2}(\phi_{\mathrm{W}} - \phi_{\mathrm{P}})\right] S_{\mathrm{ew}} \\ & + \left[\frac{|v_{\mathrm{s}}| + v_{\mathrm{s}}}{2}(\phi_{\mathrm{S}} - \phi_{\mathrm{SS}}) + \frac{v_{\mathrm{s}} - |v_{\mathrm{s}}|}{2}(\phi_{\mathrm{P}} - \phi_{\mathrm{N}}) + \frac{|v_{\mathrm{n}}| - v_{\mathrm{n}}}{2}(\phi_{\mathrm{N}} - \phi_{\mathrm{NN}})\right. \\ & \left. + \frac{|v_{\mathrm{n}}| + v_{\mathrm{n}}}{2}(\phi_{\mathrm{S}} - \phi_{\mathrm{P}})\right] S_{\mathrm{ns}}\Bigg\}, \end{aligned} \tag{43}$$

where a full upwind scheme is solved implicitly.

4. COMPUTATIONAL RESULTS AND DISCUSSION

4.1. Lid-driven cavity flow

The schematics of this test case, which has been extensively studied [13,17,18], are shown in Figure 2. The numerical results obtained by Ghia *et al.* [13] with a higher order scheme, have been taken here as a reference solution. Four uniformly spaced grids were used: 20×20, 40×40, 80×80 and 160×160 cells. The Reynolds number is defined as $Re = UL/v$ where U and L are the velocity and the length of the moving wall on the top of the cavity, respectively.

Figures 3–5 show the profiles $u(y)$ at $x = 0.5$ and $v(x)$ at $y = 0.5$ for Reynolds number $Re = 1000$ obtained with the CU (Figure 3), TVD (Figure 4) and SOU (Figure 5) schemes. All residuals were reduced below the value 10^{-8}.

Simulations with the TVD scheme were performed with the Khosla and Rubin deferred correction method. This is certainly the most efficient iterative method; in fact, accounting implicitly for the second-order TVD upwind contribution as given by Equations (22)–(26), it does not run successfully unless the relaxation parameters are small enough to ensure a diagonally-dominant coefficient matrix. This is shown in Figure 6, which reports in the case of the 40×40 grid the zone where the ratio $(|A_{\mathrm{P}}|/r_v)/(\Sigma_{NB}\,|A_{NB}|)$ is less than one for different

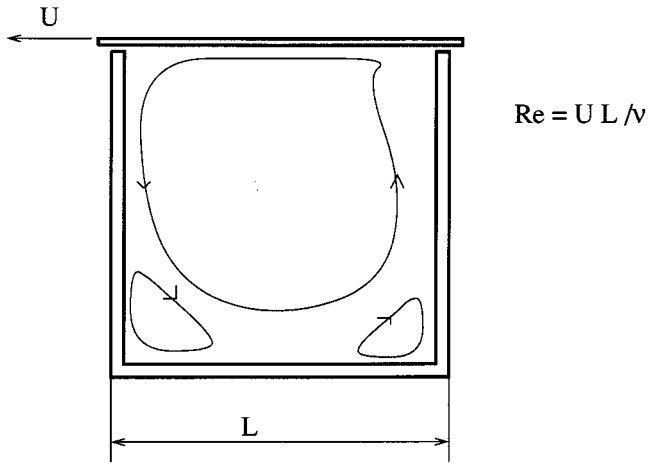

Figure 2. Schematics of the plane lid-driven cavity problem.

values of r_u and r_v. Figure 7 shows the convergence histories of the total mass residual for the different values of the relaxation parameters; the relaxation parameters had to be decreased to 0.2 in order to get a converged solution. The convergence history is also reported in the figure, obtained by dynamically selecting the optimum values of the relaxation parameters, i.e. the largest ones which can give a diagonally-dominant coefficient matrix over the whole flowfield, as given by relation (31). The history of such relaxation parameters during the iterative process is shown in Figure 8.

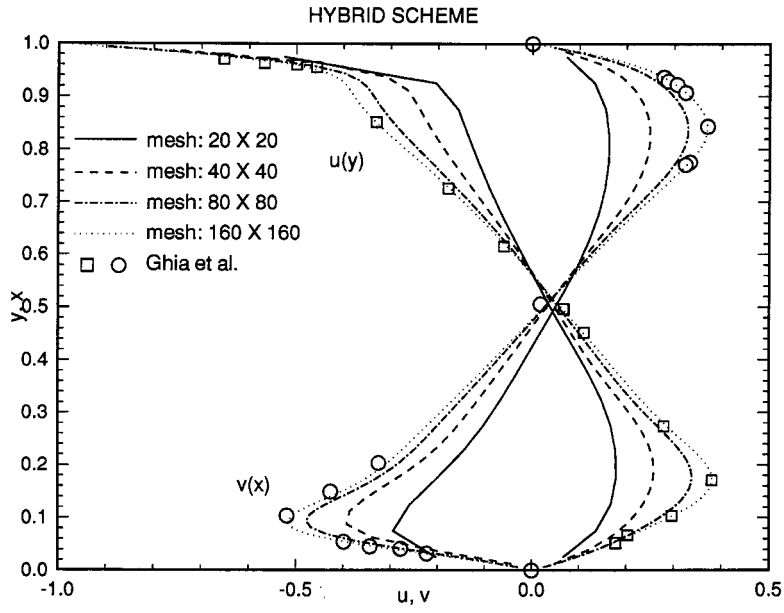

Figure 3. Lid-driven cavity. $u(0.5, y)$ and $v(x, 0.5)$ profiles obtained with the CU scheme.

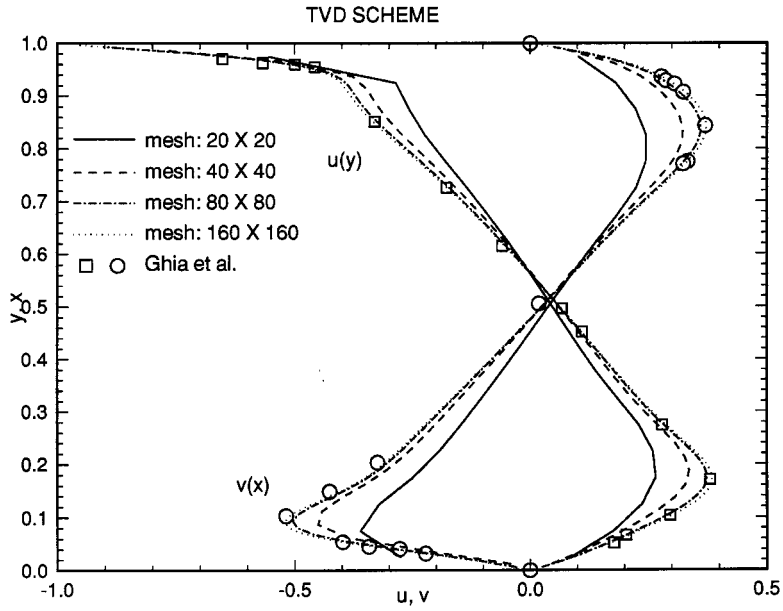

Figure 4. Lid-driven cavity. $u(0.5, y)$ and $v(x, 0.5)$ profiles obtained with the TVD scheme.

The SOU scheme was run using Khosla and Rubin's procedure. In this case the procedure shows great robustness and takes less iterations to reach convergence than the more implicit method given by Equations (32)–(37); e.g. in the case of the 40×40 grid the algorithm given

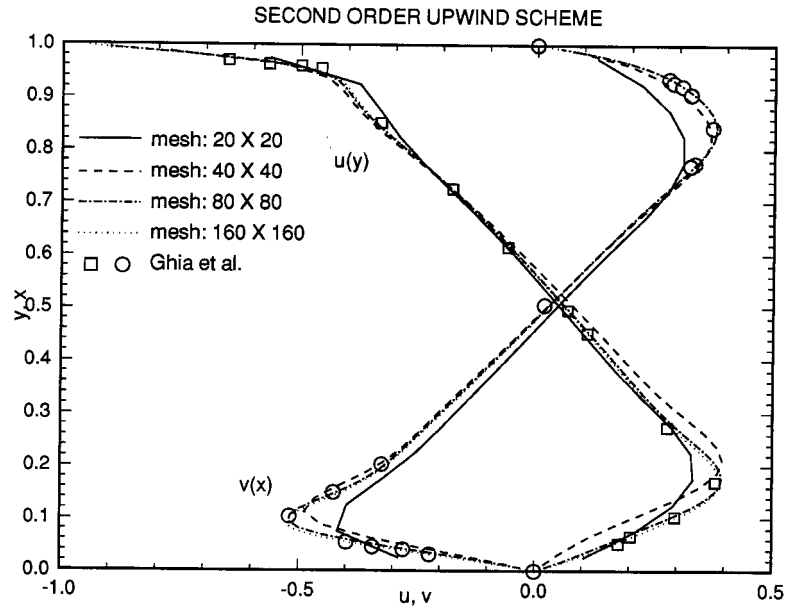

Figure 5. Lid-driven cavity. $u(0.5, y)$ and $v(x, 0.5)$ profiles obtained with the SOU scheme.

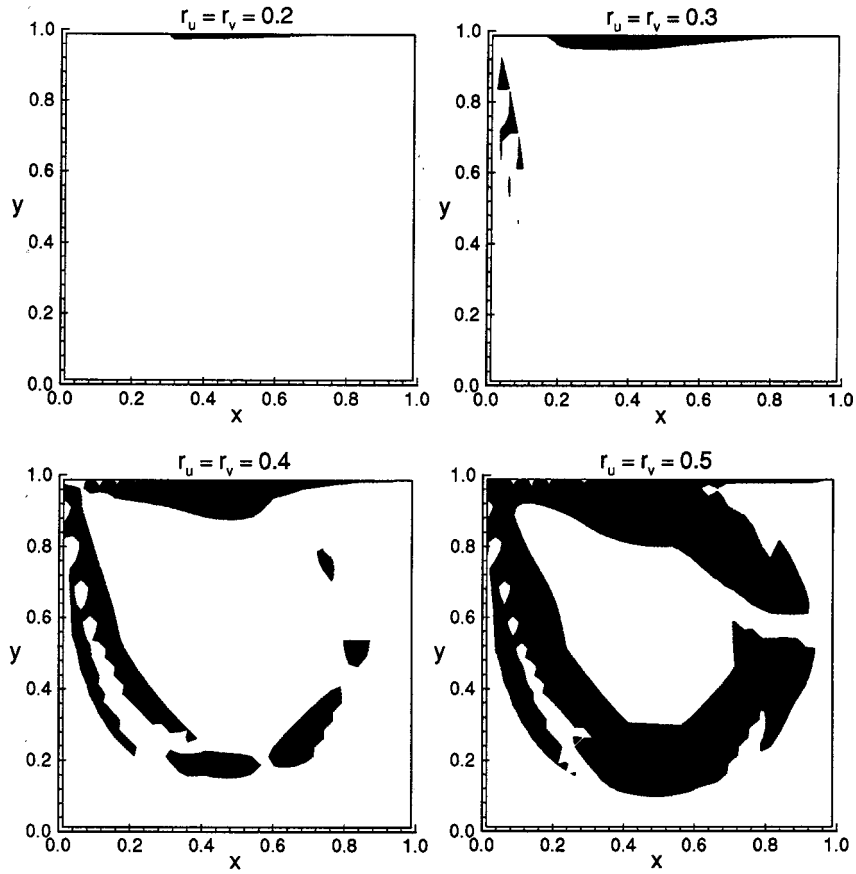

Figure 6. Lid-driven cavity. Zones (black) where the coefficient matrix in the v conservation equation is not diagonally-dominant.

by Equations (32)–(37) converges to the same residual in about 4600 iterations, while Khosla and Rubin's procedure needs about 3800 iterations.

The CU scheme gives the Ghia solution only with the finest 160×160 grid. The TVD and SOU schemes, however, can reproduce the Ghia solution with the 80×80 grid. Furthermore, it is interesting to observe that for $x < 0.5$ the $u(y)$ profile using the SOU scheme converges toward the Ghia solution in a non-monotonic way, whereas the trend is monotonic for the CU and TVD schemes.

The calculations show that the SOU and TVD schemes are robust; no numerical oscillations are generated even when using the SOU scheme, which is not monotonicity-preserving as is the TVD scheme.

Figure 9 shows the convergence histories in terms of total mass residual for the three discretization schemes, with use of the Khosla and Rubin method for the TVD and SOU schemes. The CU scheme always needs a smaller number of iterations to converge than the TVD and SOU schemes. The grid-independent solution using the CU scheme is obtained on the 160×160 grid in nearly 18 000 iterations, while this position can be reached on the 80×80 grid with the SOU scheme in nearly 10 000 iterations and with the TVD scheme in nearly 7000 iterations.

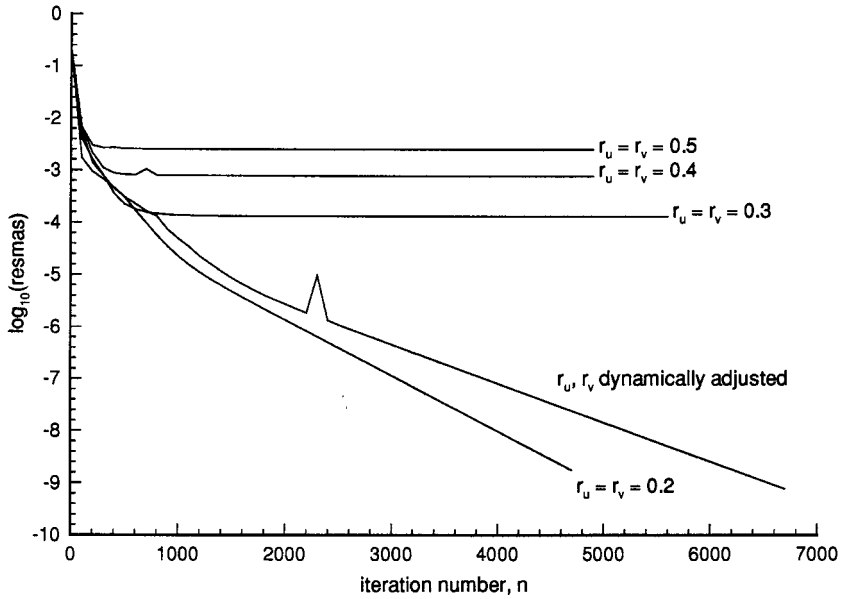

Figure 7. Lid-driven cavity. Convergence histories for different relaxation parameters obtained with TVD scheme and implicit treatment of second-order contribution (grid: 40×40).

Since one iteration on the 160×160 grid takes about four times the CPU time necessary for one iteration on the 80×80 grid, the total CPU time to obtain a grid-independent solution with TVD scheme is $18\,000 \times 4/7000 \simeq 10$ times less than the CPU time necessary with the CU

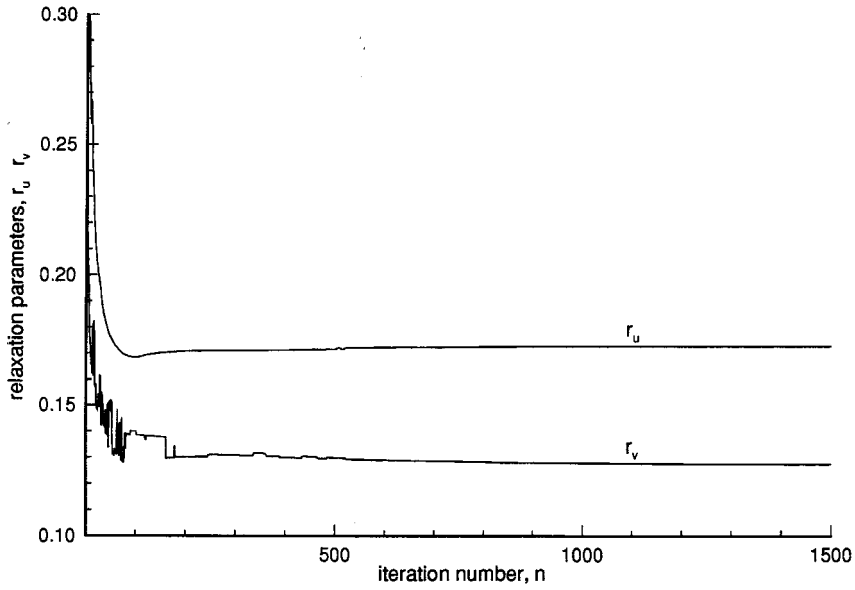

Figure 8. Lid-driven cavity. Relaxation parameters r_u, r_v dynamically adapted during iterations to obtain diagonally-dominant coefficient matrices.

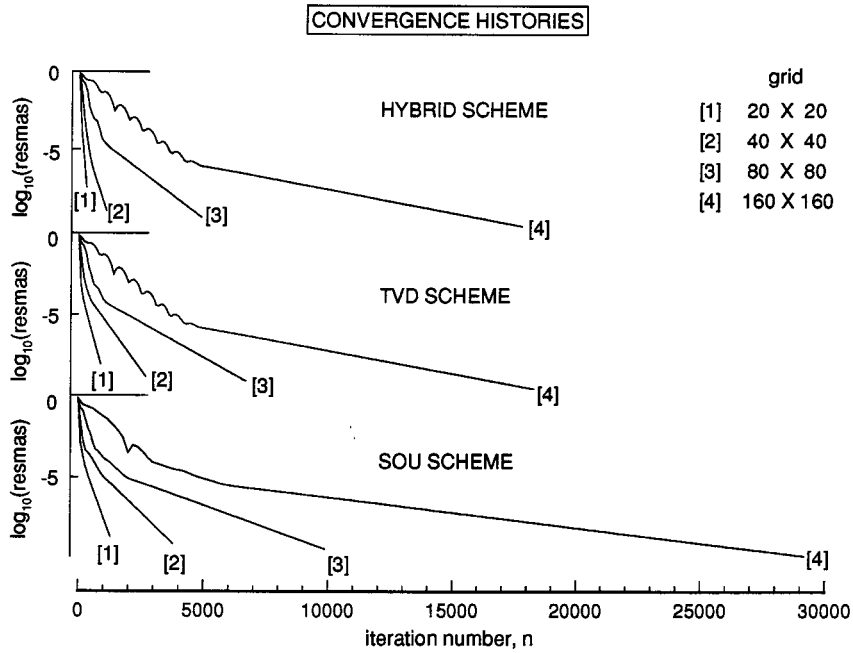

Figure 9. Lid-driven cavity. Convergence history with the CU, TVD and SOU schemes (Khosla and Rubin's method used).

scheme. The CPU time needed to obtain a grid-independent solution with the SOU scheme is $18\,000 \times 4/10\,000 \simeq 7$ times less.

4.2. *Backward facing step*

The second case considered is the two-dimensional laminar backward facing step, experimentally studied by Armaly *et al.* [14]. The calculations were performed at Reynolds numbers ranging from $Re = 100$ to 800.

The schematics of this test case are shown in Figure 10. The domain was divided into two blocks. Two grids were considered: in the second block, the coarse grid has 64×32 cells and the fine one has 128×64 cells. The grids are compressed near the inlet and uniformly spaced in the y-direction.

Two recirculation zones are present in the flow domain; a large one just downstream of the step and a smaller one, which appears starting from $Re \approx 450$, on the wall opposite to the step.

The simulations were performed with all the three discretization schemes described in the previous section. The mass and momentum components residuals were reduced below the value 10^{-5}.

Figures 11 and 12 show the reattachment length x_1 downstream of the step obtained with the two grids (the calculations on the 128×64 grid were performed starting from $Re \approx 450$). The numerical results obtained by Kim and Moin [19] using the fractional step method and a second-order scheme on a 100×100 grid are also shown. This length has been determined as

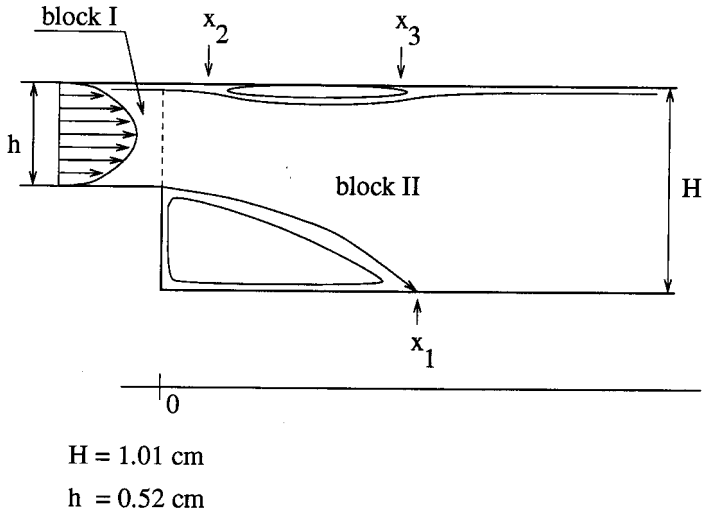

Figure 10. Schematics of the laminar backward facing step problem.

the point on the first row of nodes near the bottom wall in the computational domain where the axial velocity component changes its sign. The CU scheme on the coarse grid predicts a reattachment length x_1, which is in agreement with the experiments until $Re \approx 300$. Starting from $Re \approx 500$, the prediction for x_1 begins to decrease, in contrast with the experimental value which increases.

The TVD and SOU schemes produce more accurate results, however, the best agreement being with the TVD scheme. On the 128×64 grid the TVD scheme performs in almost the same way as on the 64×32 grid, showing that for such schemes the coarse grid is sufficient to get grid-independent results. The CU scheme does not produce sufficiently accurate results, even on the finest mesh.

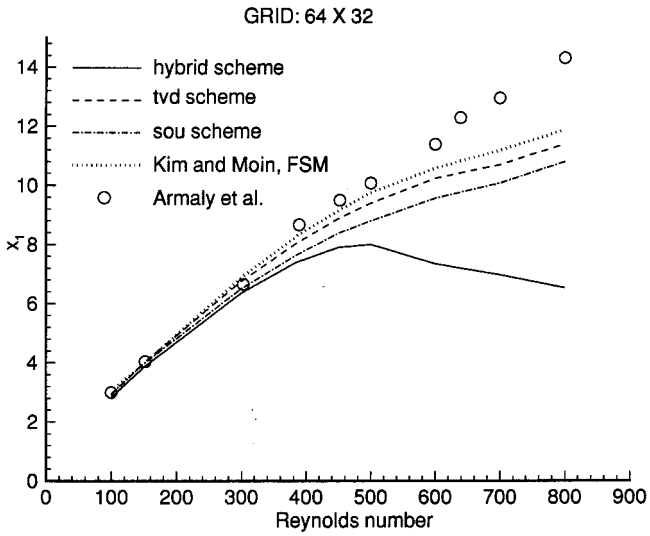

Figure 11. Backward facing step. Reattachment length x_1 downstream of the step. Grid 64×32.

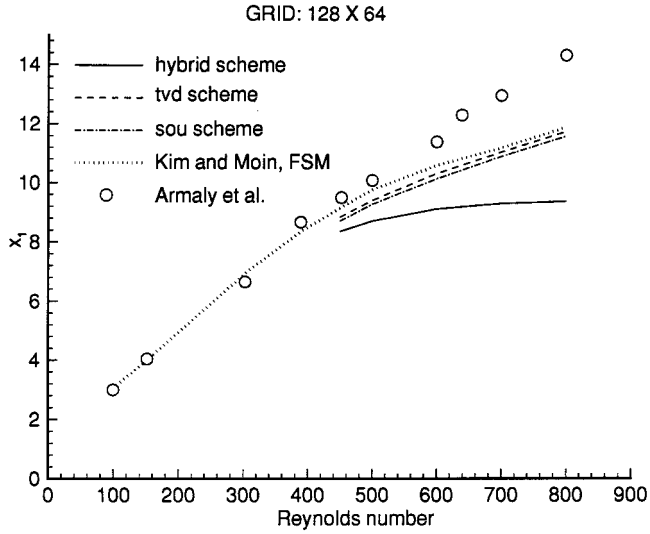

Figure 12. Backward facing step. Reattachment length x_1 downstream of the step. Grid 128×64.

Figures 13 and 14 show the position of the recirculation zone at the wall opposite to the step. Also, in this case it is confirmed that the coarse grid gives a grid-independent solution when using the TVD scheme; using the CU scheme a grid independent solution is not obtained even on the fine grid. The agreement with experiments when using the TVD scheme is fair.

Starting from $Re = 400$, the experiments show some three-dimensional flow structure; this might explain the disagreement between experiments and calculations (which are two-dimensional) even using the finest mesh and the second-order schemes.

In nearly all cases, the Khosla and Rubin deferred correction procedure has been applied, assuming the relaxation parameters in the transport equations for the momentum components

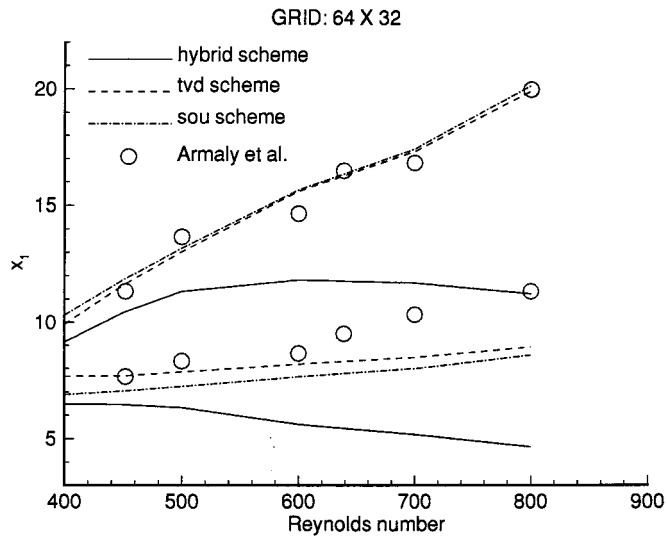

Figure 13. Backward facing step. Position of the recirculation zone at the wall opposite to the step. Grid 64×32.

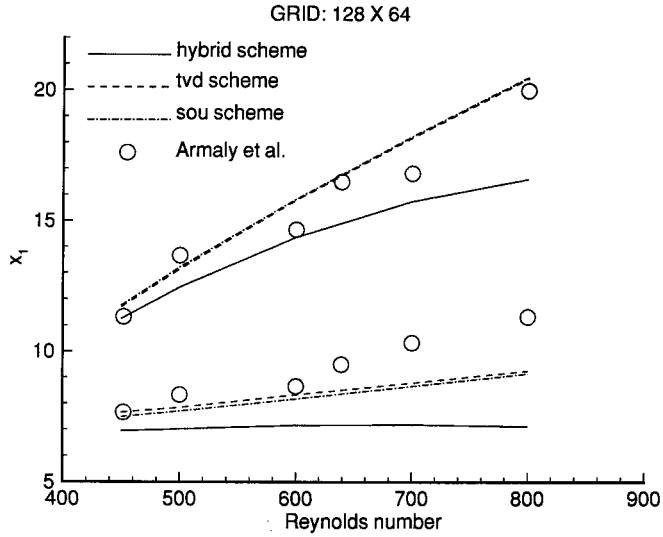

Figure 14. Backward facing step. Position of the recirculation zone at the wall opposite to the step. Grid 128×64.

are equal to 0.5. For $Re \geq 600$ and using the TVD scheme, it was not possible to lower all residuals below the value 10^{-5}, even with the relaxation parameters set equal to 0.1. Figure 15 shows the convergence histories for the u-residual obtained in these two cases. The same calculation was performed with the TVD scheme and the algorithm given by Equations (22)–(26); this one does not converge if the relaxation parameters are set equal to 0.5. In this case, the coefficient matrix is not diagonally-dominant over the whole field. Therefore, the calculation was performed (as also done for the case of the lid-driven cavity flow) with the

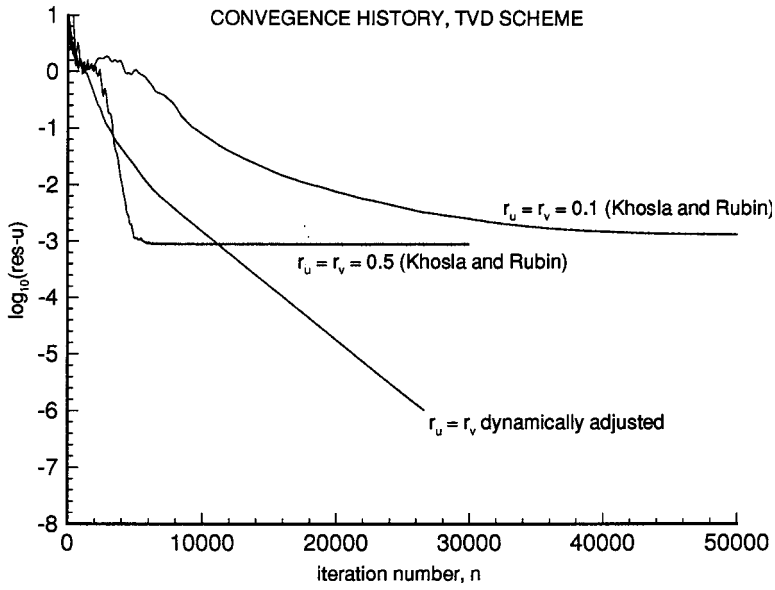

Figure 15. Backward facing step. Convergence histories obtained with TVD scheme on the 128×64 grid.

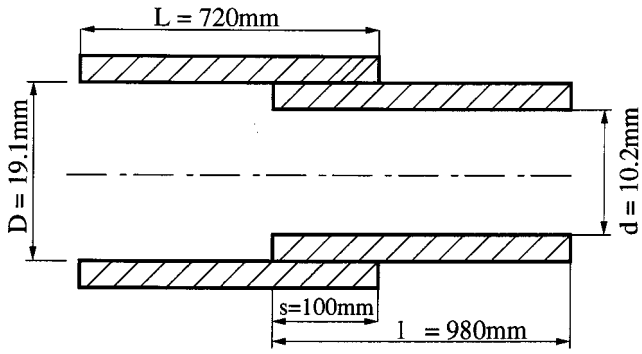

Figure 16. Schematics of the pipe with sudden contraction.

relaxation parameters dynamically adapted to values capable of ensuring diagonal dominance everywhere, as given by Equation (31). Figure 15 shows that in this case convergence can be achieved in about 20 000 iterations.

4.3. Pipe flow with a sudden contraction

The third test case considered is the flow in a pipe with the sudden contraction of cross sectional area, experimentally studied by Durst and Loy [15]. The schematics of this test case are shown in Figure 16. The case relative to Reynolds number $Re_D = UD/\nu = 372$ was considered for simulation in this case, where U is the volumetric average axial velocity at the inlet. The flow domain was divided into two blocks, one upstream (dimension 100×9.55 mm) and one downstream (dimension 100×5.01 mm) of the sudden contraction. Two grids were considered: a fine grid composed of 64×64 (upstream block) and 64×32 cells (downstream block), and a coarse grid composed of 32×32 cells (upstream block) and 32×16 (downstream block). The grid density was increased in the region of the sudden contraction where steep variations in velocities were expected and all residuals were reduced below 10^{-5}.

Figures 17–19 show radial profiles of the axial velocity component at six sections in the pipe obtained with the three discretization schemes. Khosla and Rubins method was used for the TVD and SOU schemes. The three schemes perform in a very similar way on the fine grid; in fact, they almost give the same results which are in very good agreement with the experiments.

The TVD performs only slightly better than the CU and SOU schemes on the coarse grid; it predicts the overshoot of axial velocity, experimentally observed just downstream of the contraction, near the pipe wall. In any case, the solution on the coarse grid cannot be considered to be grid-independent.

5. CONCLUSIONS

The second-order TVD and SOU schemes were applied to three laminar test cases, two of which had large recirculation zones. The comparison with previous numerical calculations for the case of the lid-driven cavity flow and with experiments for the case of the backward facing step, shows that these schemes perform much better than the standard hybrid central upwind (CU) scheme. In fact, using the CU scheme, in order to get the same accuracy of the TVD scheme in the case of the lid-driven cavity flow, the mesh had to be doubled, resulting in an order of magnitude increase in CPU time.

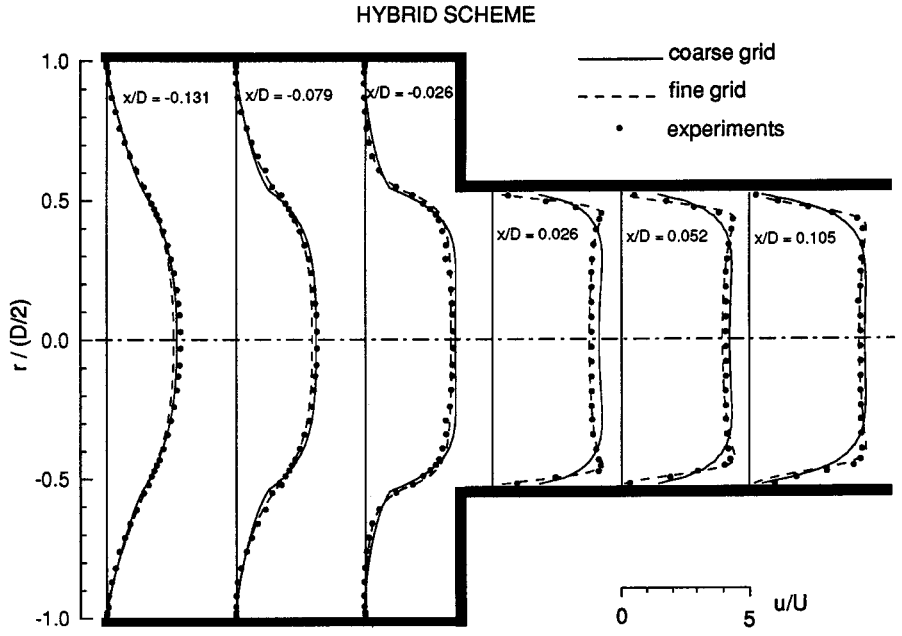

Figure 17. Pipe flow. Radial profiles of the axial velocity component $\tilde{u}$ at six sections in the pipe. CU scheme used.

To have an unconditionally diagonally-dominant coefficient matrix, the deferred correction procedure by Khosla and Rubin was adopted. Nevertheless, it was found that the TVD scheme using Khosla and Rubin's method, may be responsible for poor convergence performance in

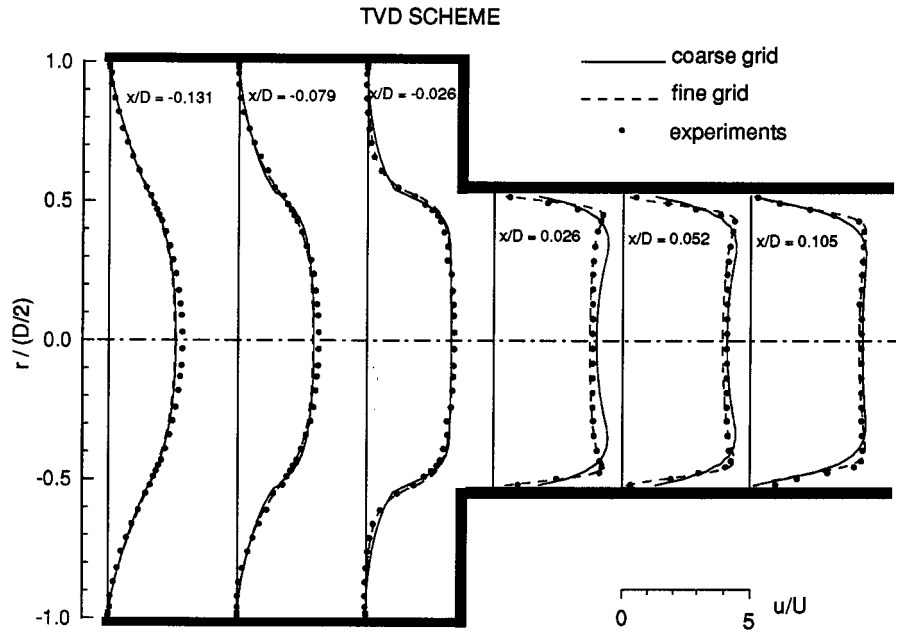

Figure 18. Pipe flow. Radial profiles of the axial velocity component $\tilde{u}$ at six sections in the pipe. TVD scheme used.

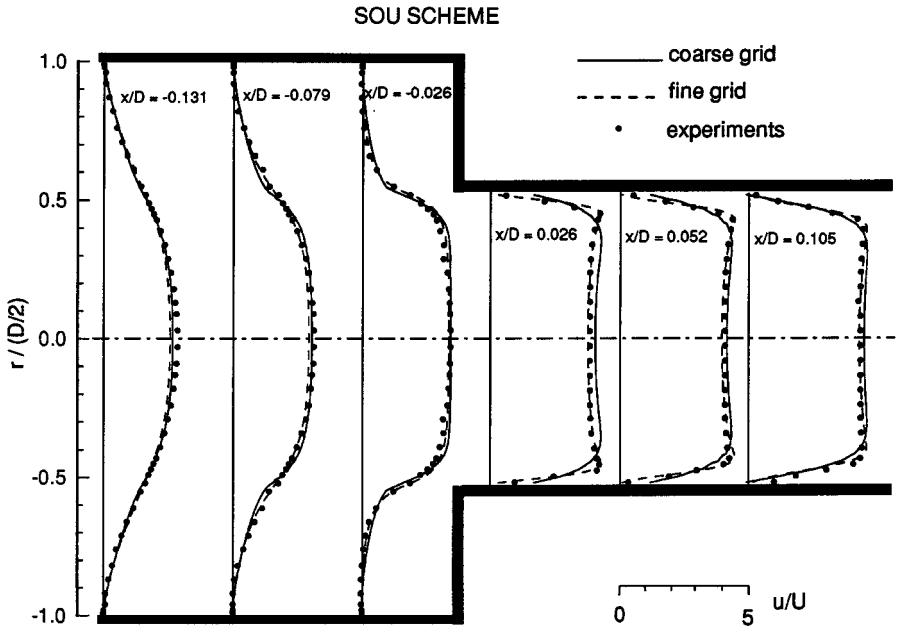

Figure 19. Pipe flow. Radial profiles of the axial velocity component $\tilde{u}$ at six sections in the pipe. SOU scheme used.

the case of the backward facing step at large Reynolds number. The method based on the implicit consideration of the TVD second-order upwind contribution, applied with relaxation parameters sufficiently low to ensure diagonal dominance, can instead reach very low residuals without any problems. Therefore, an adaptive (dynamic) determination of the optimum relaxation parameters (i.e. the maximum values capable of ensuring a diagonally-dominant coefficient matrix over the whole flowfield) has been devised and successfully tested with the TVD scheme.

The flow in a pipe with the sudden contraction of cross sectional area was also tested. In this case no large differences between the CU, the TVD and SOU schemes were observed.

ACKNOWLEDGMENTS

This work was financially supported by the Sardinian Regional Government and ENEACRE Casaccia (Rome).

REFERENCES

1. S.V. Patankar, *Numerical Heat Transfer and Fluid Flow*, Hemisphere Publishing Corporation, New York, 1980.
2. B.P. Leonard, 'A stable and accurate convective modelling procedure based on quadratic upstream interpolation', *Comput. Methods Appl. Mech. Eng.*, **19**, 59–98 (1979).
3. R.F. Warming and R.M. Beam, 'Upwind second-order difference schemes and applications in aerodynamic flows', *AIAA J.*, **14**, 1241–1249 (1976).
4. P.H. Gaskell and A.K.C. Lau, 'Curvature-compensated convective transport: SMART, a new boundedness-preserving transport algorithm', *Int. j. numer. methods fluids*, **8**, 617–641 (1988).
5. B.P. Leonard and S. Mokhtari, 'Beyond first-order upwinding; the ULTRA-SHARP alternative for non-oscillation steady-state simulation of convection', *Int. j. numer. methods eng.*, **30**, 729–766 (1990).
6. A. Harten, 'High resolution schemes for hyperbolic conservation laws', *J. Comput. Phys.*, **49**, 357–393 (1983).
7. R.J. Le Veque, *Numerical Methods for Conservation Laws*, Birkhäuser Verlag, Basel, 1990.

8. W.P. Jones, 'Turbulence modelling and numerical solution methods for variable density and combusting flows', in P.A. Libby and F.A. Williams (eds), *Turbulent Reacting Flows II*, Academic Press, New York, 1992, pp. 375–474.
9. P.L. Roe, 'Some contributions to the modeling of discontinuous flows', *Lecture Notes Appl. Math.*, **22**, 163–193 (1985).
10. B. Van Leer, 'Towards the ultimate conservative difference scheme II. Monotonicity and conservation combined in a second order scheme', *J. Comput. Phys.*, **14**, 361–370 (1974).
11. F. Biagioli, 'Modeling turbulent combustion with probability density function methods', *Ph.D. Thesis*, Mechanics and Aeronautics Dept., University of Rome I (in Italian), 1995.
12. P.K. Khosla and S.G. Rubin, 'A diagonally dominant second-order accurate implicit scheme', *Comput. Fluids*, **2**, 207–209 (1974).
13. U. Ghia, K.N. Ghia and C.T. Shin, 'High-*Re* solutions for incompressible flow using the Navier–Stokes equations and a multigrid method', *J. Comput. Phys.*, **48**, 387–411 (1982).
14. B.F. Armaly, F. Durst, J.C.F. Pereira and B. Schonung, 'Experimental and theoretical investigation of backward-facing step flow', *J. Fluid Mech.*, **127**, 473–496 (1983).
15. F. Durst and T. Loy, 'Investigations of laminar flow in a pipe with sudden contraction of cross sectional area', *Comput. Fluids*, **13**, 15–36 (1985).
16. C.M. Rhie and W.L. Chow, 'Numerical study of the turbulent flow past an airfoil with trailing edge separation', *AIAA J.*, **21**, 1525–1532 (1983).
17. G. De Vahl Davis and G.D. Mallinson, 'An evaluation of upwind and central difference approximations by a study of recirculating flows', *Comput. Fluids*, **4**, 29–43 (1976).
18. W. Shyy, S. Thakur and J. Wright, 'Second-order upwind and central difference schemes for recirculating flow computation', *AIAA J.*, **30**, 923–932 (1992).
19. J. Kim and P. Moin, 'Application of a fractional-step method to incompressible Navier–Stokes equations', *J. Comput. Phys.*, **59**, 308–323 (1985).

